Need predictive capability for plasma performance

Since the plasma and wall exchange the entire plasma content many times even in short pulse discharges, this obviously requires, to start at the beginning, a predictive capability for the plasma-wall exchange

The problem of "voodoo confinement"

carbonization
boronization
lithium application
.....

<u>Many inter-related processes are involved, some poorly characterized</u>

- Extrinsic impurity properties (screening properties of ergodic divertor)
  basic processes: atomic rates; JHU / LLNL / Frascati collaboration

- Intrinsic impurity generation processes (relation between lab-scale and observed rates)
  basic processes: chemical sputter , RES, hydrocarbon break-up

- Hydrogenic particle exchange mechanisms (role of energetic CX fluxes, films)
  basic processes: ‘hard’, ‘soft’ films; Jacob, von Keudell experiments

- AT physics: impurity dynamics (Er and ripple)

ornl

Integrating issue: physics focus is steady-state fusion plasma

--> with the D-T cycle, sufficiently rapid helium exhaust must be attained, and the requirement is more stringent when additional impurities are present

Wolf-Reiter criterion

To attain
$n\tau_E T_i = 10^{22}$ (keV s / m^3)
ρ_{WR} must
be lower than →

$\rho_{WR} \equiv \tau_{He^*} / \tau_E$

$\tau_{He^*} \equiv \tau_{He} / (1 - R_{He})$

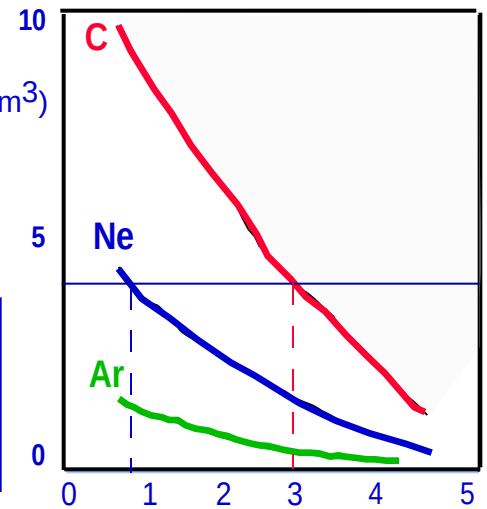

typical present values
ρ_{WR} *~ 4-10 (ELMy H-mode)*
> 15 (strong ITB)

Adapted from U. Samm et al, Proc. 22nd EPS, Bournemouth and D. Reiter, G. Kleva, G. Wolf Nucl Fus 1992

Non-helium impurity fraction $f_{i,max}$ (%)

	0	0.9	1.8	C
ΔZ_{eff}	0	2.5	5	Ne
	0	10	20	Ar

This integrating requirement inextricably couples
- plasma-wall particle exchange
- intrinsic and extrinsic impurity properties
- erosion

C O D E S

SOL Monte Carlo impurity transport (3D)

BBQ: 3-D, velocity space

Collision model like LIM, WBC, ERO codes
but, includes 3-D, toroidal magnetic geometry

Background parameters assumed (n_e, ,λ_n, T_e, λ_T)

[local D^+ flux amplification, sheath
electrostatic (es) field, E_{SOL}]

$M_Z\, dV_Z/dt = -F_{friction} - F_{es}$
+ random // and diffusion

$F_{friction} = -M_Z (V_{SOL} - V_Z) / \tau_s$; $F_{es} = Ze\, E_{SOL}$

$F_{//}$ = Random // diffusion, $D_{//} = (8E_Z/3\pi M_i)\, \tau_{//}$
F = Random anomalous diffusion (D)

$dE_Z/dt = (kT_i - E_Z)/\tau_T + W_{friction} + W_{es}$

Molecular processes: Erhardt-Langer, Allman-Ruzic hydrocarbon break-up rates

Atomic processes (ionization, recombination, D_0 charge exchange) for D, C, He, Ne, N, Ar

Birth gyro-collisions with surface

Core impurity transport (1-D, time)

MIST (developed by R. Hulse - PPPL)
1-D (radial) , t multi-species
impurity transport code

Atomic physics:
- ADPAK (original)
- STRAHL (K. Behringer)
- JHU/LLNL/Frascati (HULLAC) collaboration (M. Mattioli)

NCLASS (developed by W. Houlberg - ORNL)
Full expressions for neo-classical fluxes with multi-species impurities

Wall thermal analysis (3-D, time)

CASTEM-2000 (developed by CEA-DEMT).

Modifications ('physics package') include:
- self-consistent heat flux (from n_e, T_e, Φ) (includes SEE, thermionic)
- local impurity redeposition heat source

Wall equilibration (1-D, time)

WDIFFUSE (ORNL)
1-D (depth into a-C:H layer) , time
multi-species wall
deposition/retention/saturation code
(combined with neutral CX calculation:
Eirene or similar)

ornl

Caveat: Edge modeling in the "ORNL - CEA collaboration"

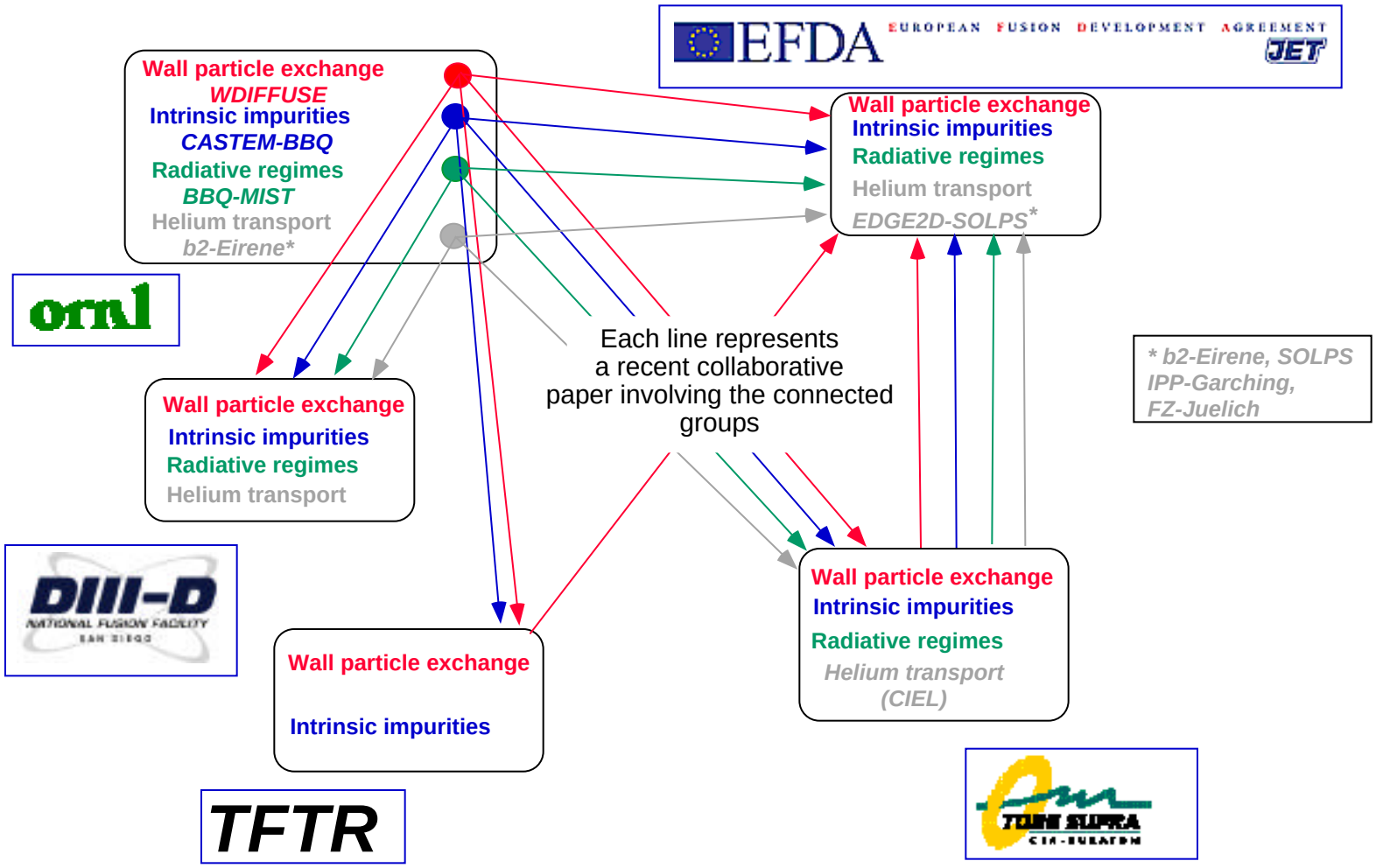

ornl

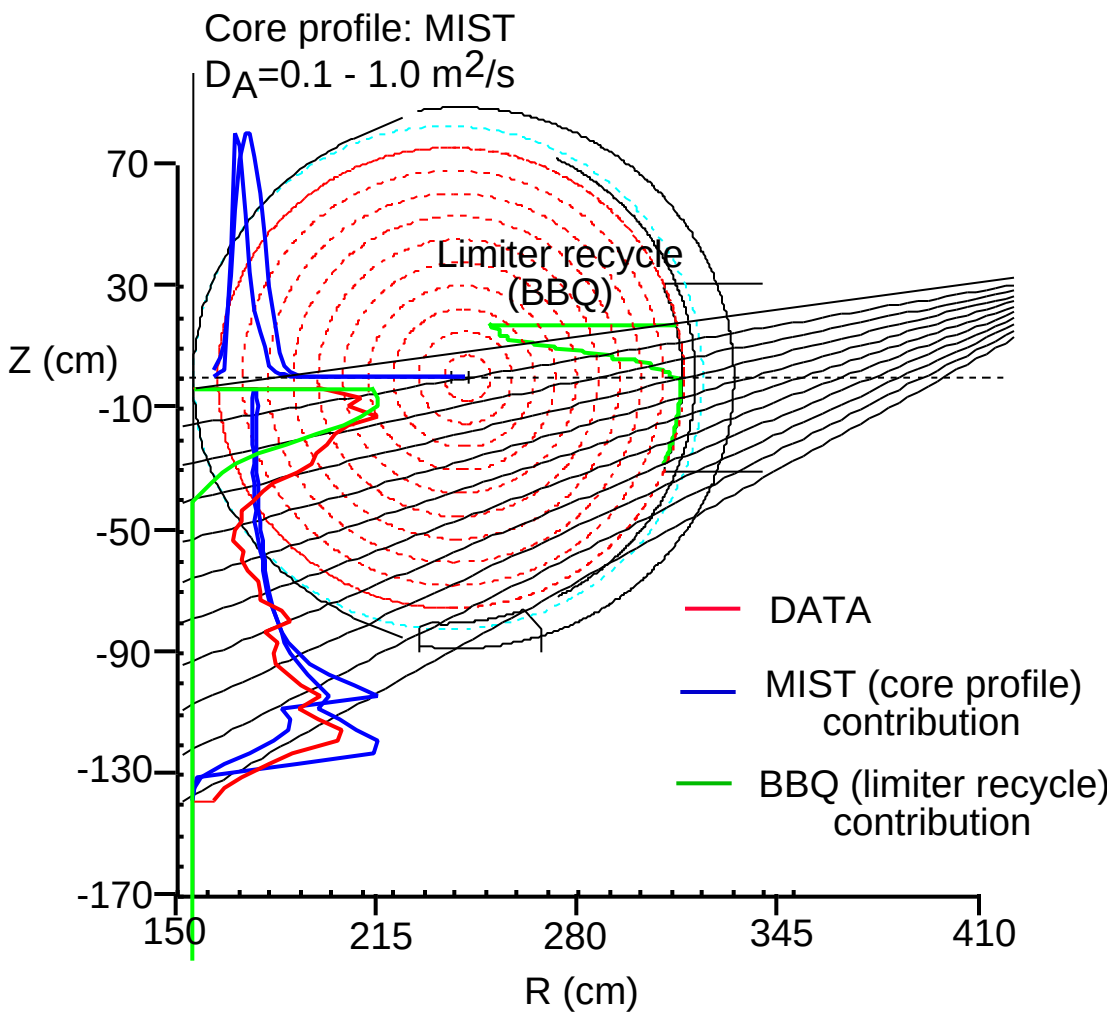

Figure 19. Contributions of symmetric (MIST) and asymmetric (BBQ) sources to duochromator signal

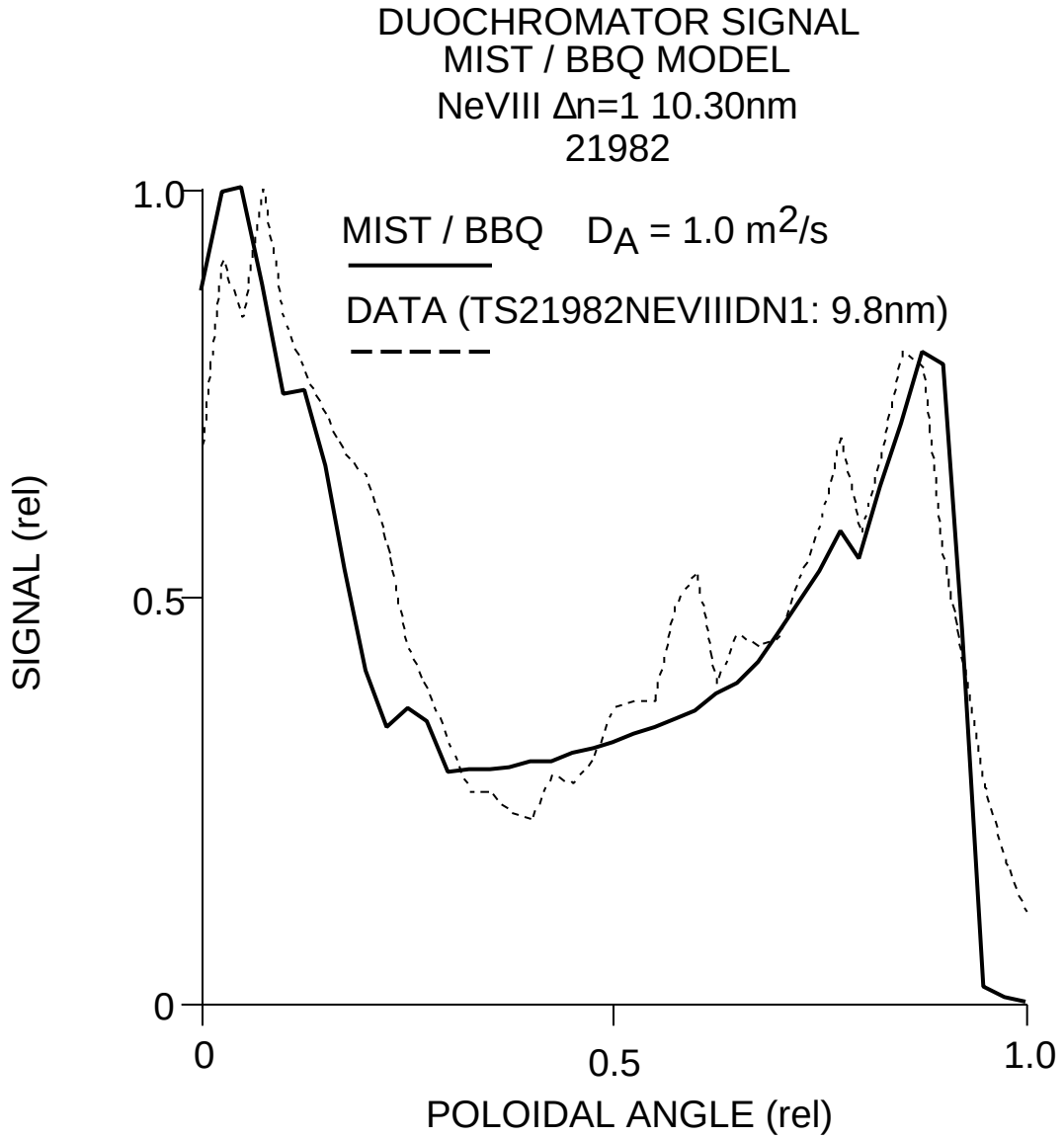

Figure 21a. MIST/BBQ predicted duochromator signal for NeVIII 10.3nm line

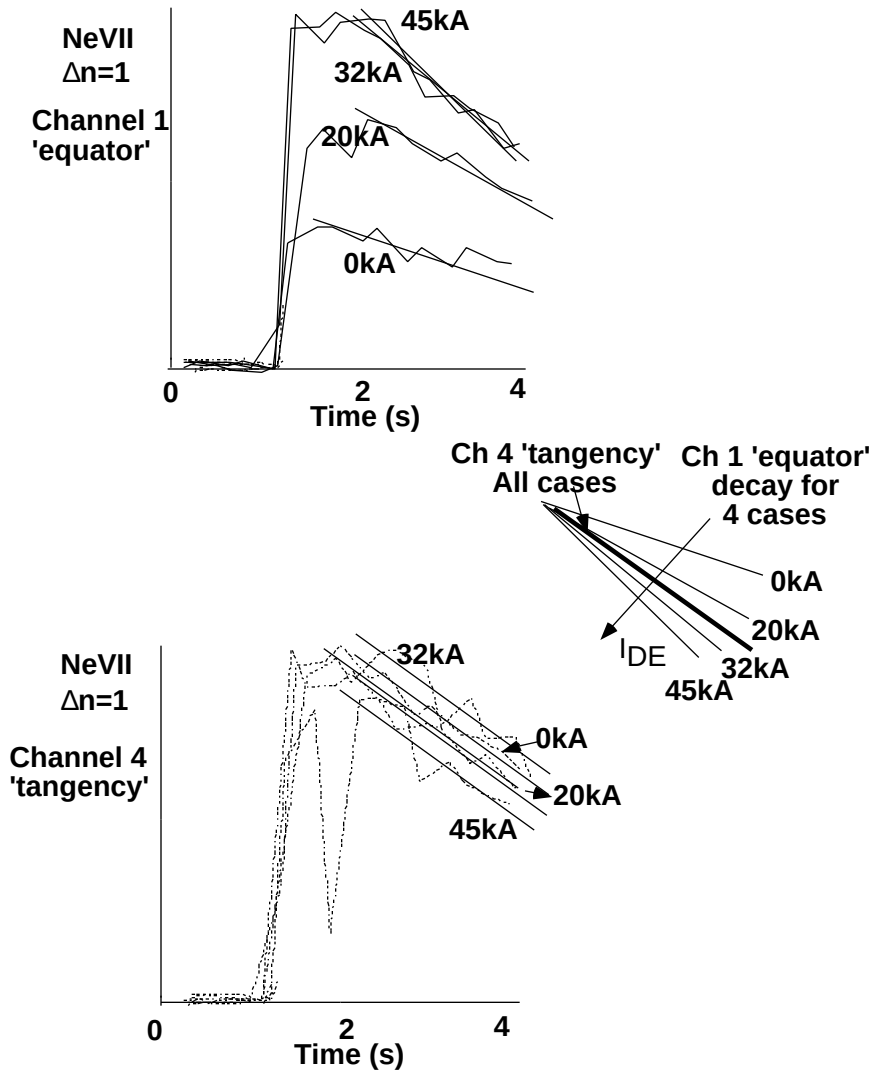

Figure 9 : Time decay for equator and tangency angles

Ne I Density : top view

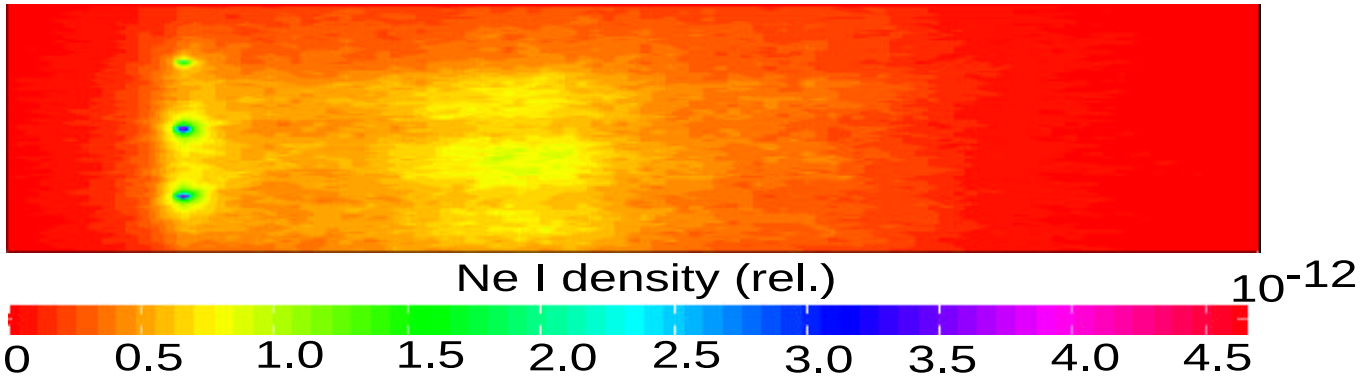

Ne I density : side view

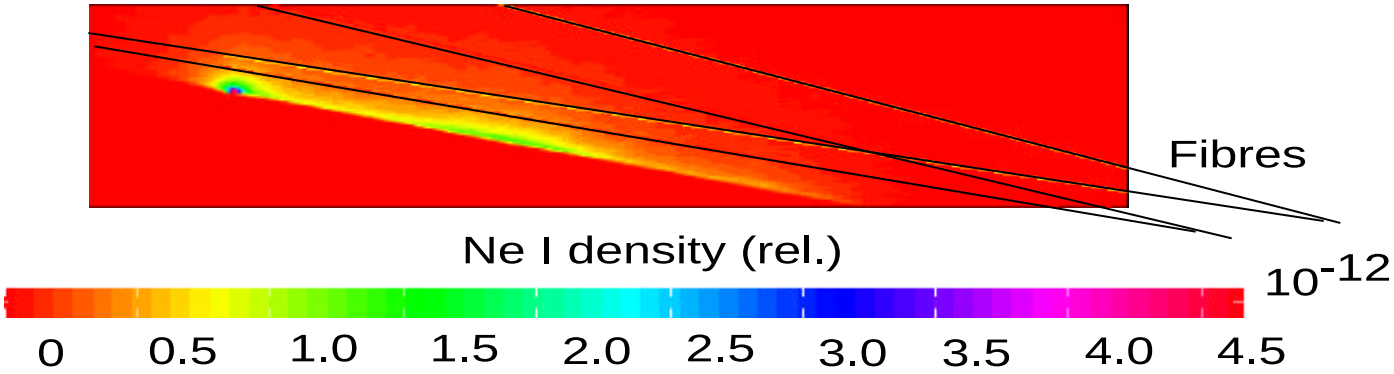

I_{DE} = 45 kA Te(L.P.) = 60 eV

ornl

BBQ simulation of Ne fibre integrals in the vicinity of the DE neutralizer for a scan in T_e

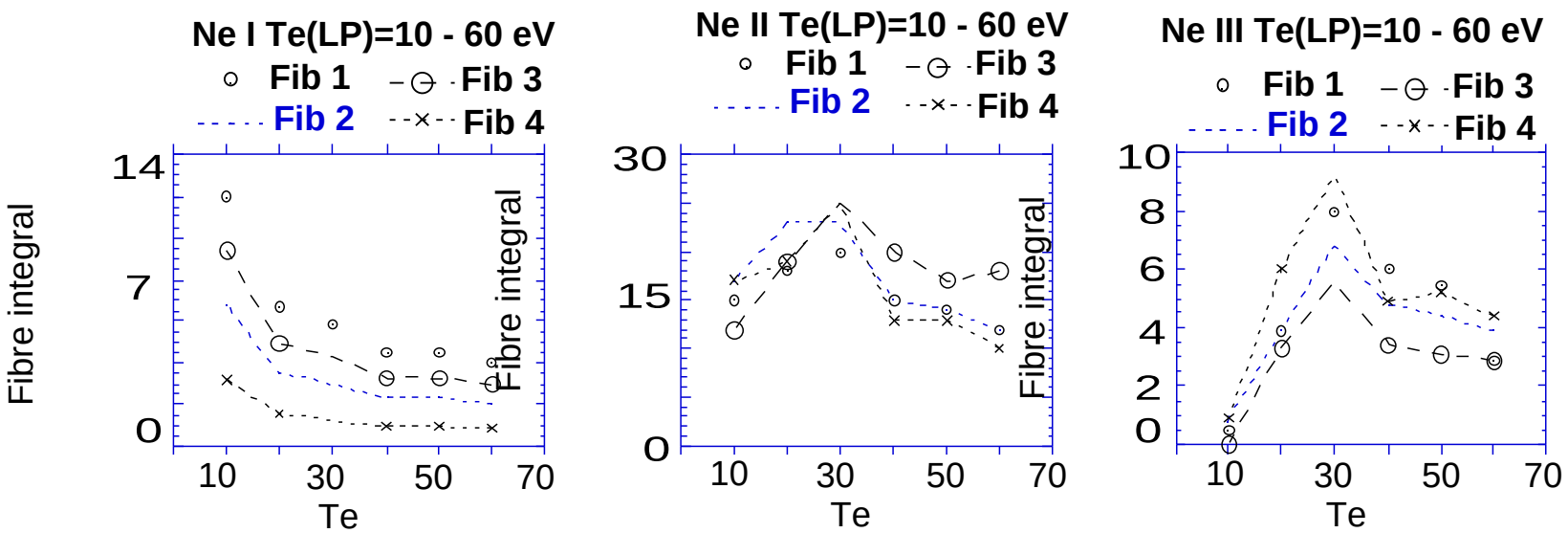

3D BBQ simulation: core penetration fraction increases as T_e(LP) decreases

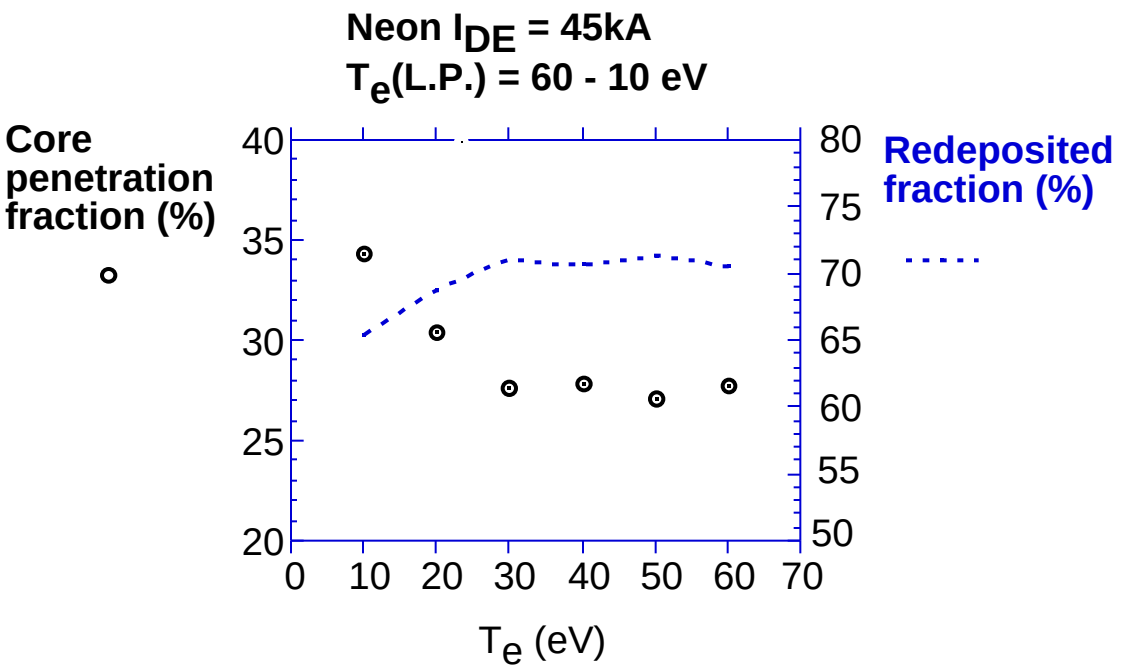

Core neon content determined by MIST / BBQ fit to SIR Ne Lyα, total radiated power using previously validated tranport model

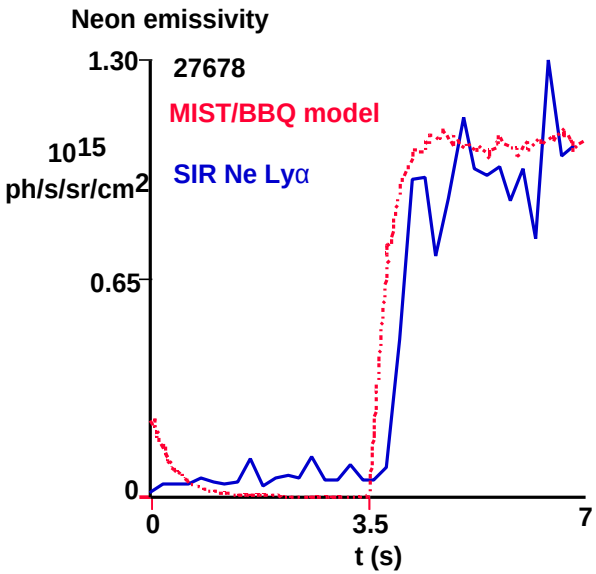

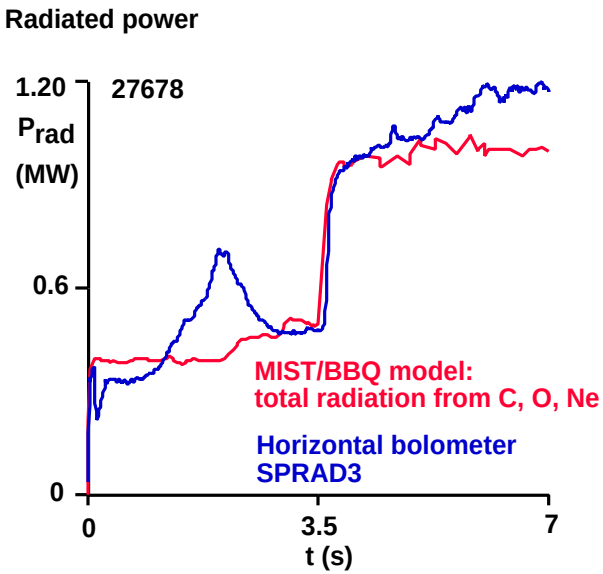

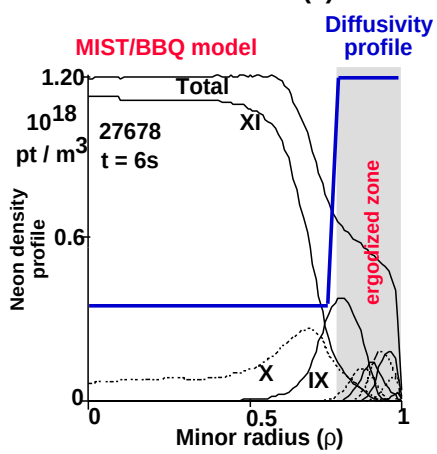

Neon density radial profile with transport model (D_A, V_A) obtained from match with 27845: CXS profiles available for C and Ne; I_{DE}=45kA)*

* W. Hess et al, EPS Buda-Pest 2000

Hybrid 1D (MIST) - 3D SOL (BBQ) model fits core VUV, SXR, Prad and (for benchmark shots) CXS data

Results from impurity decay, SS high Prad experiments with ergodic divertor show elevated transport localized in the ergodic region

This explains the ELM-like decoupling of impurity fluxes from divertor plates and core impurity content

R. Guirlet, J. Hogan, C. DeMichelis et al
IAEA Sorrento, 2000

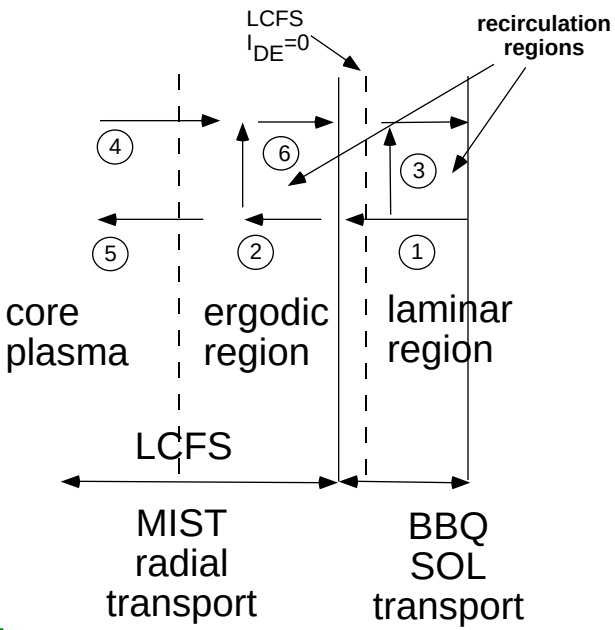

Radial impurity fluxes for N and Ne deduced from high radiation regimes experiments using the ergodic divertor

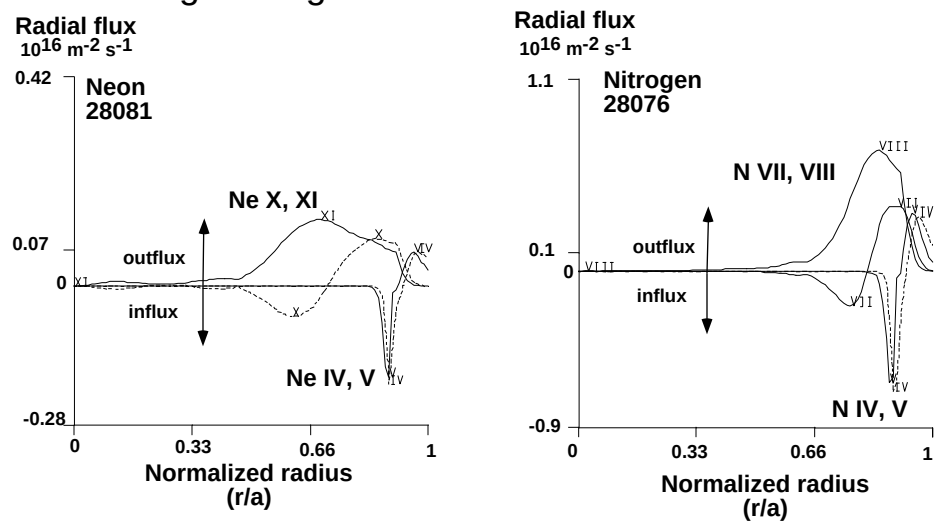

Numerical experiment:

Assumed increase in SOL influx (BBQ) countered by increased efflux from ergodic region -

core region unchanged

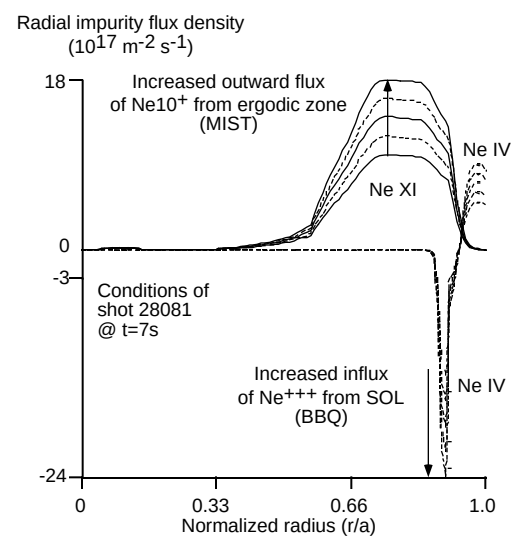

DIII-D intrinsic impurities before/after new tile installation

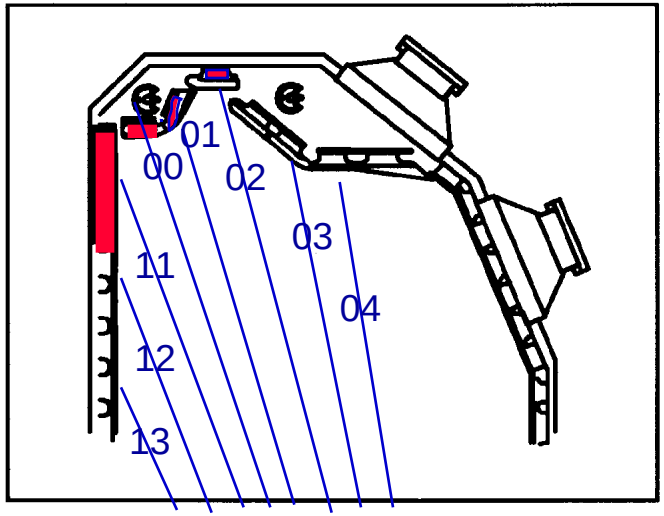

Filterscope (schematic)

Some evidence of T-dependent processes

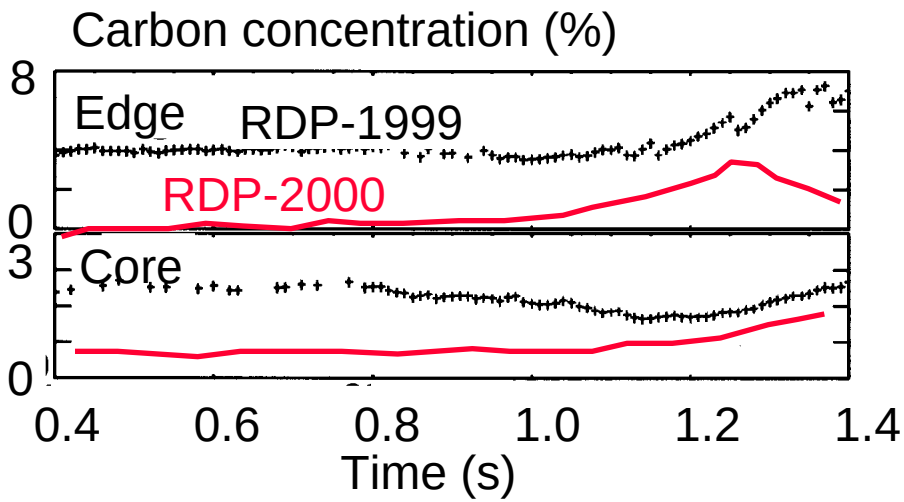

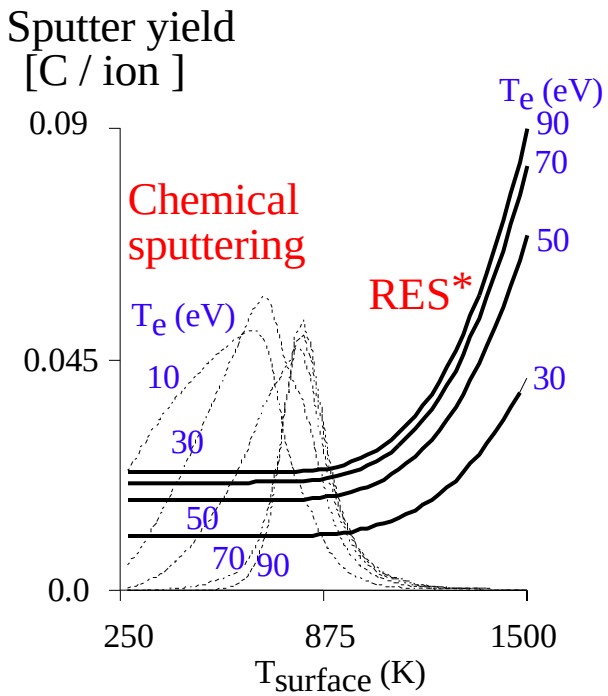

*Radiation-Enhanced Sublimation

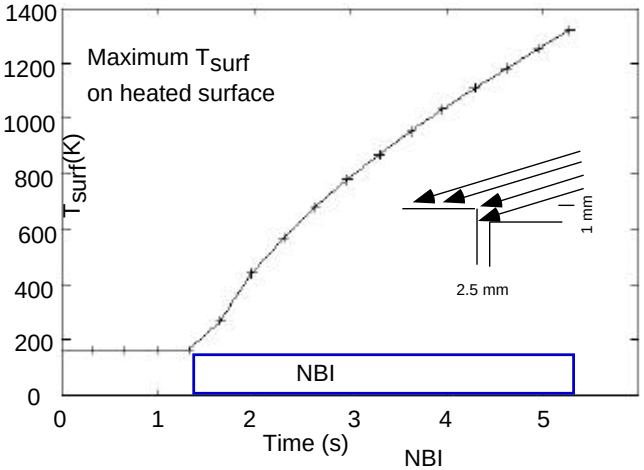

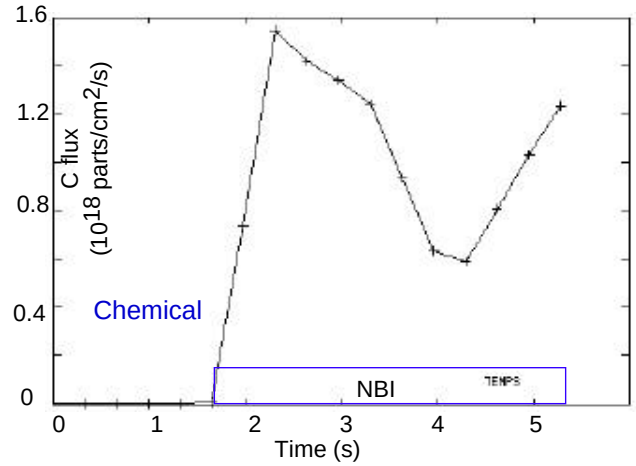

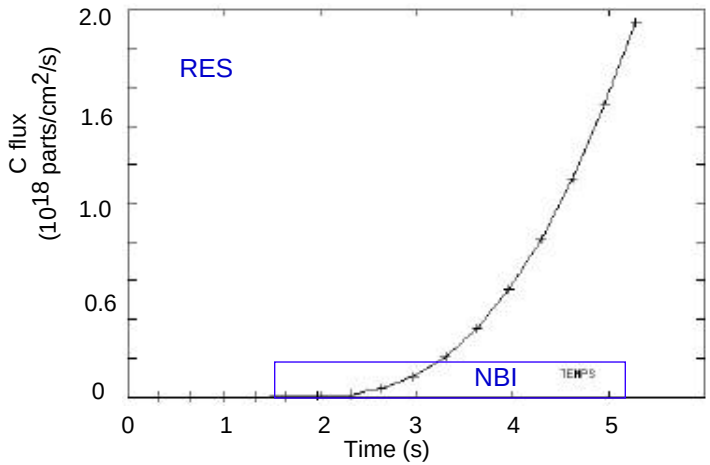

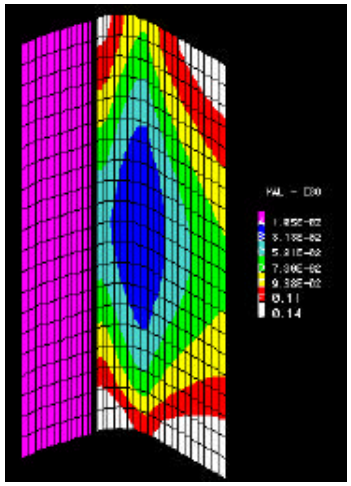

Y_{chem} @ t ~ 4s
when T_{max} = 1010K

$Y_{chem}^{min} = 1.\ 10^{-2}$

$Y_{chem}^{max} = 0.14$

Experimental set-ups

Neutraliser area behind the pumped limiter

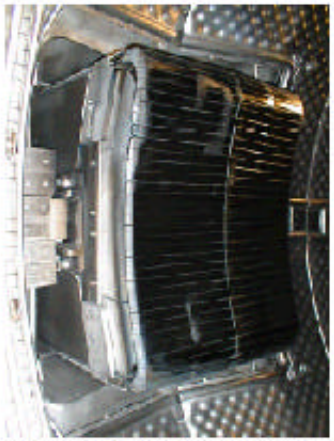

Fig. 2 : Pumped limiter made out of pyrolitic graphite

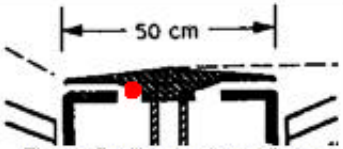

Fig. 5 : Profile of pumped limiter and observation point

Plasma conditions as in the neutraliser of the next stage.

Simultaneous ex-vessel observation by an optical fibre transparent up to 2 µm and an Infrared camera at 3.9 µm for reference.

Calorimetric ripple protection plate

Fig. 3 : Ripple protection plate and main observation point

Fig. 4 : In vessel optics

In-vessel test: 5 near infrared fibres, optics and feedthroughs.

Aim to measure energy and spatial distribution of ripple ions.

Calorimetry as reference.

Common for both set-ups:

60 m relay by fibres,

2 spectrometers (3.7 and 0.2 nm resolution) with 256 channel detectors working between 0.85 and 1.6 µm, and a single channel detector at 1.95 µm.

R. Reichle et al, J Nucl Mater (to appear)

ornl

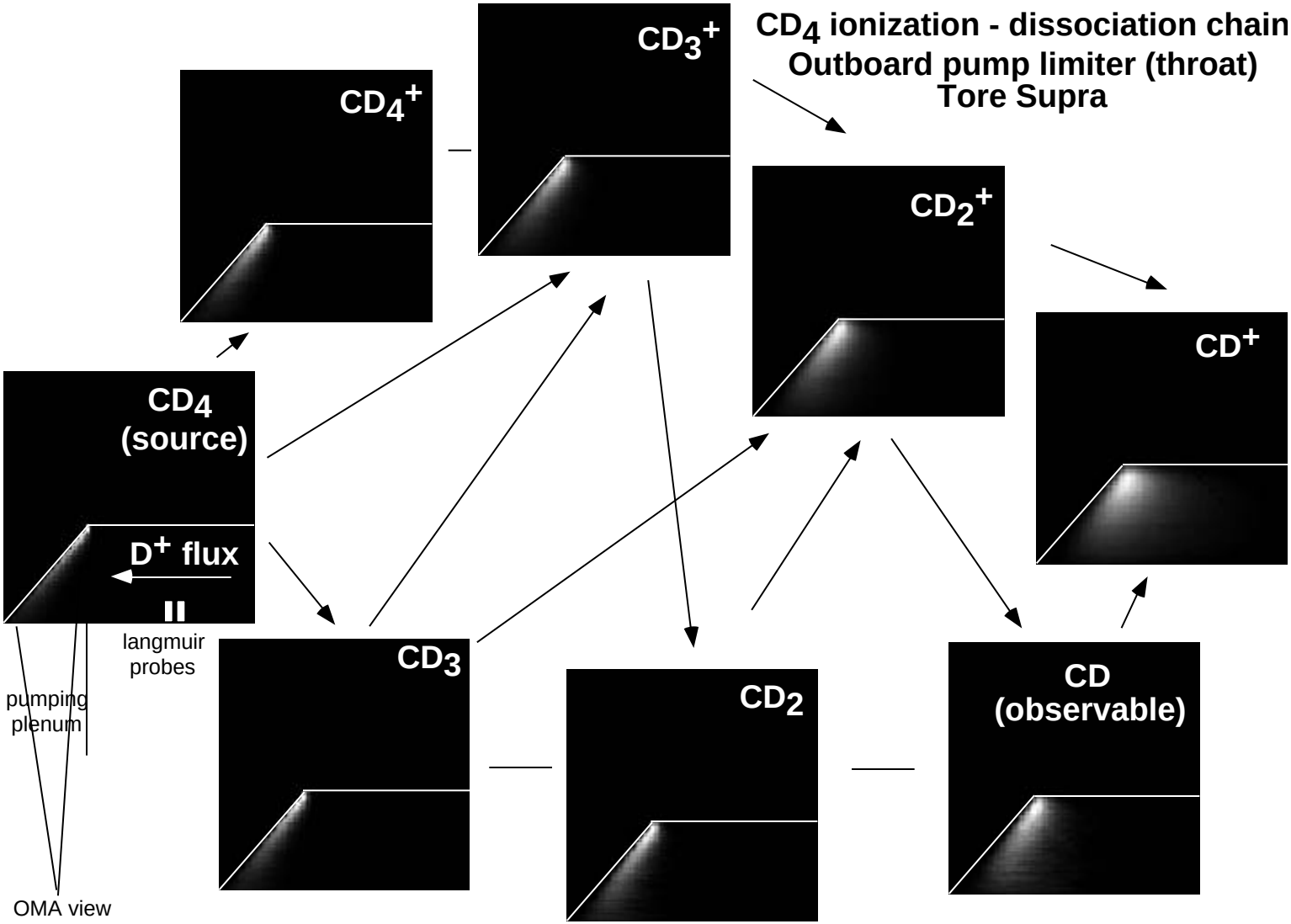
CD4 ionization - dissociation chain
Outboard pump limiter (throat)
Tore Supra
CD4+
CD3+
CD2+
CD+
CD4
(source)
D+ flux
langmuir
probes
pumping
plenum
OMA view
CD3
CD2
CD
(observable)

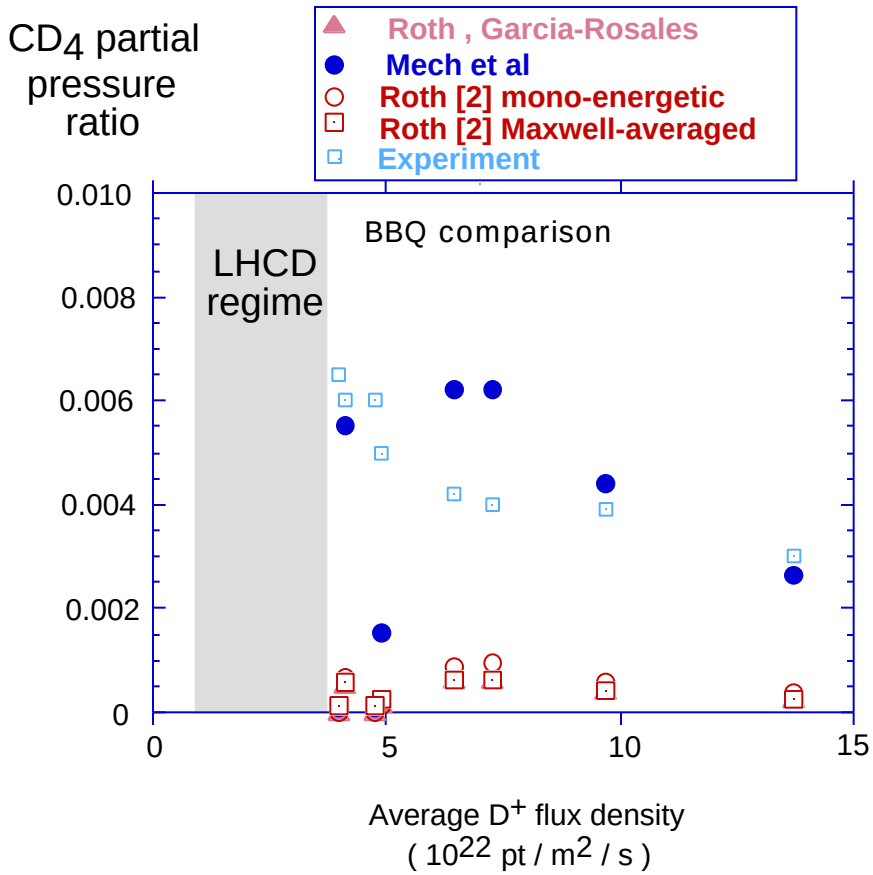

Comparison of predictions using (1) Roth, Garcia-Rosales, (2) Mech et al, (3) mono-energetic and (4) Maxwell-averaged rates from [2], with measured partial pressures.

R. Ruggieri, E. Gauthier, J. Hogan et al
J Nucl Mater '99

Measurements Part 5: Surface condition of targets

Target behind the limiter

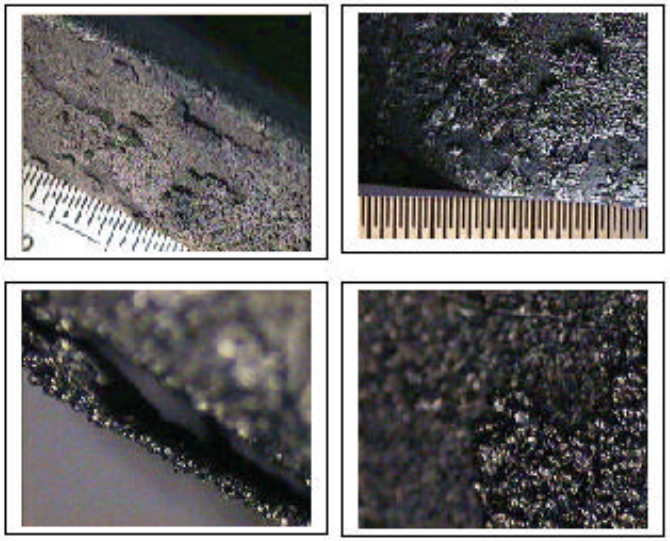

Fig. 14: Macro-photos of flakes on the target area behind the limiter. The lower row of pictures has a 7 times larger magnification than the upper ones.

Target on ripple protection plate

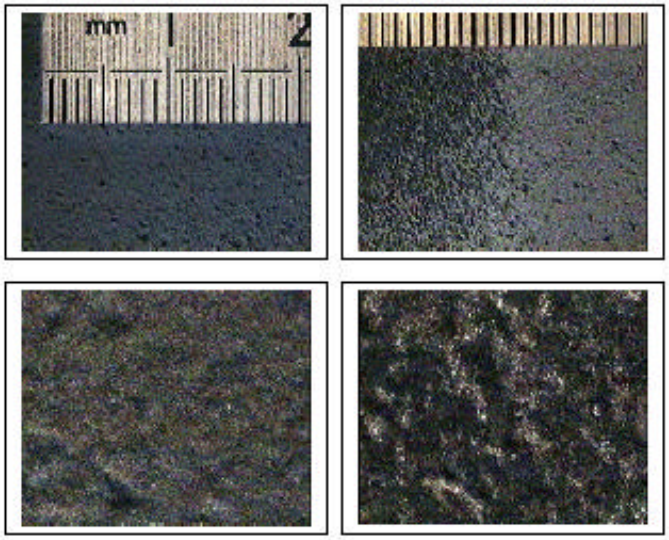

Fig. 15: Macro-photos of the target at the ripple protection plate on the right, and of a unchanged reference area on the left. The lower row of pictures has a 7 times larger magnification than the upper ones.

Detached flakes behind the limiter !

Thickness up to 70 μm.

No flakes on the ripple plate, but small grain change of target zone : localised darkening.

R. Reichle et al, J Nucl Mater (to appear)

ornl

Role of films in plasma-wall exchange

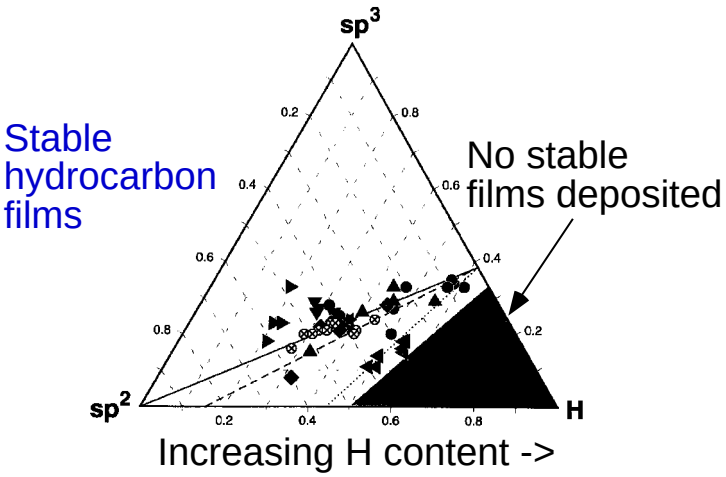

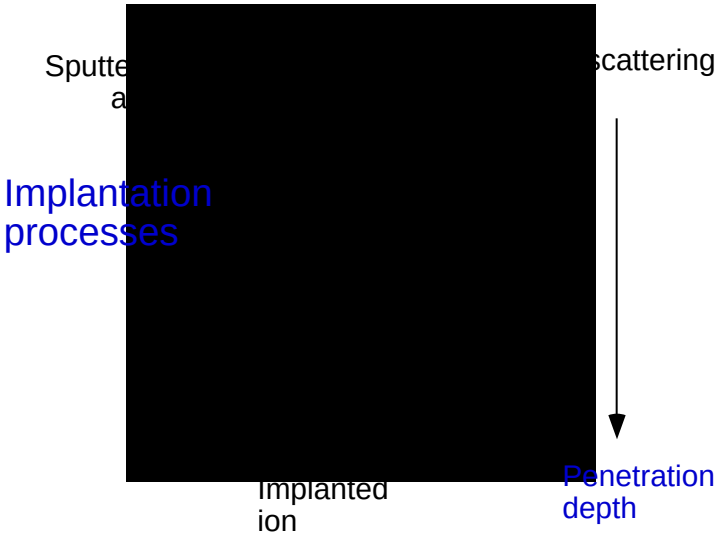

Wide range of stable hydrocarbon films, properties depending on H (D/T) content

Content, in turn, depends on previous plasma history

Size of reservoir for retention is proportional to penetration depth

Depth, in turn, depends on film position in 'hard'-'soft' spectrum

W. Jacob

"Surface reactions during growth and erosion of hydrocarbon films"

Thin Solid Films 326 (1) 1998

ornl

Test of semi-empirical wall models using WDIFFUSE for JET D-T change-over (41677)

D. Hillis, J. Hogan, J. Ehrenberg et al

Phys Plas 1999

solute concentrations

$$\frac{dc_s^D}{dt} = -k_0 (c_s^D)^2 - k_0 c_s^D c_s^T - \frac{dc^D}{dt} + \Sigma^D$$

$$\frac{dc_s^T}{dt} = -k_0 (c_s^T)^2 - k_0 c_s^D c_s^T) - \frac{dc_t^T}{dt} + \Sigma^T$$

trapped concentrations

$$\frac{d}{dt} c_t^D = k_{s,t} c_s^D \left(1 - \frac{(c_t^D + c_t^T)}{c_{t,s}}\right) - k_{t,s} c_t^D$$

$$- k_d c_t^D (\Sigma^D + \Sigma^T)^{1/2} - \sigma_{dt} c_t^D (\Sigma^D + \Sigma^T)$$

$$\frac{d}{dt} c_t^T = k_{s,t} c_s^T \left(1 - \frac{(c_t^T + c_t^D)}{c_{t,s}}\right) - k_{t,s} c_t^T$$

$$- k_d c_t^T (\Sigma^D + \Sigma^T)^{1/2} - \sigma_{dt} c_t^T (\Sigma^D + \Sigma^T)$$

volume recombination rate -> timescale

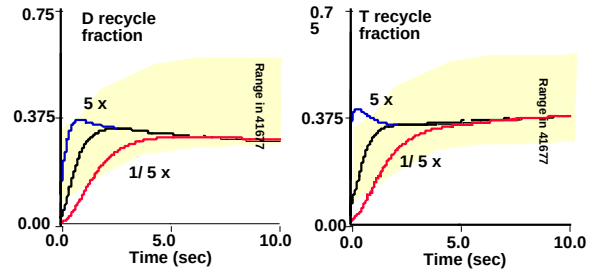

particle-induced detrapping rate-> magnitude of plasma-induced isotope exchange

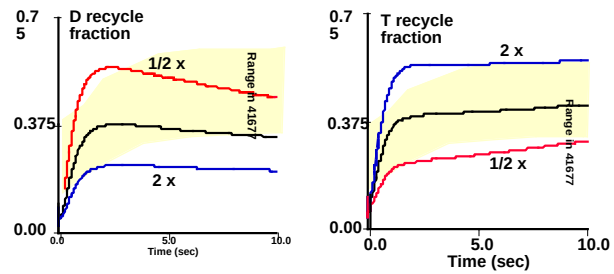

Implantation flux density, depths from Eirene modeling

Exptl range of T recycle (KT5P)

MODEL	Recombination	Trapping	Thermal detrapping	Particle-induced detrapping	
	k_0 (cm^3/s)	k_{st} (s^{-1})	$k_{t,s}$ (s^{-1})	k_d ($cm^{3/2}\ s^{-1/2}$)	σ_{dt} (cm^2)
Ehrenberg	$2.5\ 10^{-21}$	10^4	0.	$6\ 10^{-13}$	-
Moeller-Scherzer	$1.2\ 10^{-18}$	10^{-4}	$1.9\ 10^{-12}$	-	$5\ 10^{-17}$
Grisolia	$1.0\ 10^{-20}$	10^2	$5\ 10^{-2}$	-	$8\ 10^{-17}$

ornl

Similarity of CD / CH band amplitudes (G. Duxbury et al) with D / H ratio of KT5P (subdivertor) partial pressures during JET D -> H change-over (48280 et seq) suggests that chemical erosion may be the physical process underlying the semi-empirical 'particle-induced desortpion

D. Hillis, J. Hogan, G. Duxbury et al
J. Nucl Mater (to be publ)

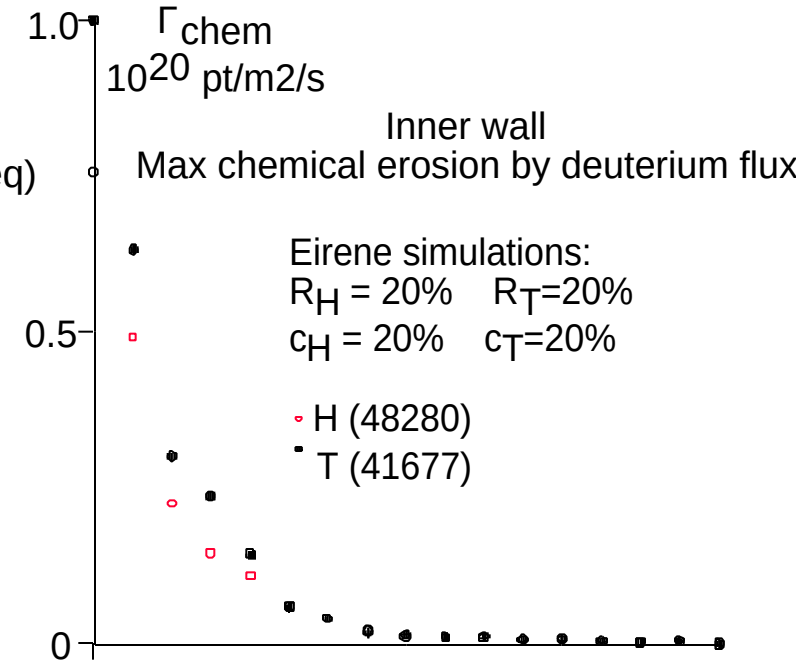

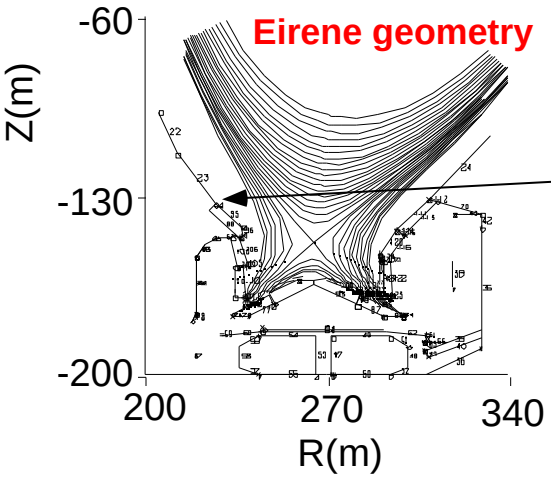

Comparison of SOL / divertor conditions in JET / TFTR

Typical TFTR SOL parameters:
(used in BBQ modeling cases)

Shot	n_e ($10^{18} m^{-3}$)	T_e (eV)
76528	9.9	660
76530A	9.3	590
76530B(OH)	3.7	200
76649	8.4	440
88615	1.2	420

Typical JET detached divertor conditions are represented (right) by EDGE2D* simulation of pulse 44028.

$n_e > 10^{20} m^{-3}$ and $T_e < 30$ eV

- EDGE2D is the JET 2-D divertor transport code
- it is coupled to the NIMBUS neutrals code (CX flux)

* thanks for help with the code to G. Corrigan, J. Spence (EFDA/ JET)

Typical JET detached divertor parameters
(EDGE2D simulation)

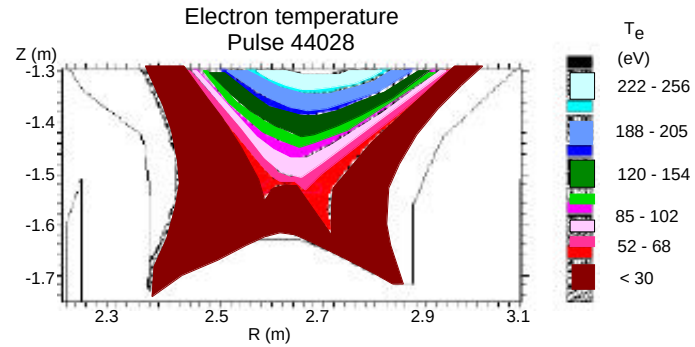

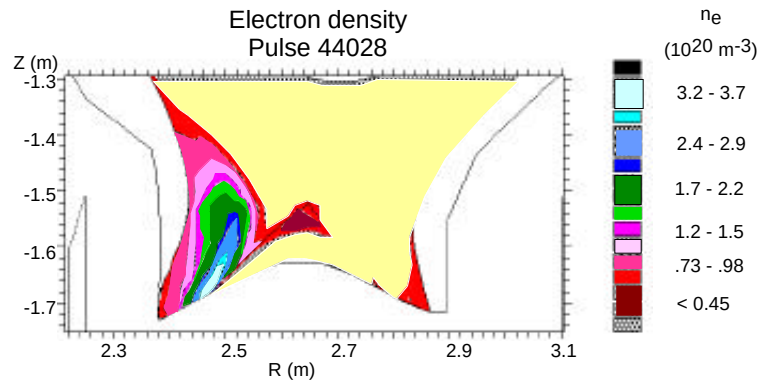

Plasma environment for TFTR / JET tritium retention experiments spans ~2 orders of magnitude

ornl

GEOMETRY MODELS

TFTR Inner Bumper Limiter
CAD model: BL-LIM.DRW
Detailed tile positions
3-D non-uniformity

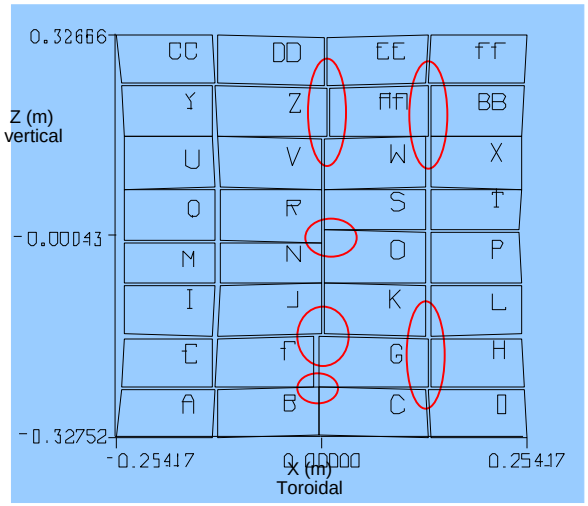

BL sector

Irregularity

TS Plasma Paroi Interne (PPI)
Analytic model*
Detailed tile positions
3-D non-uniformity

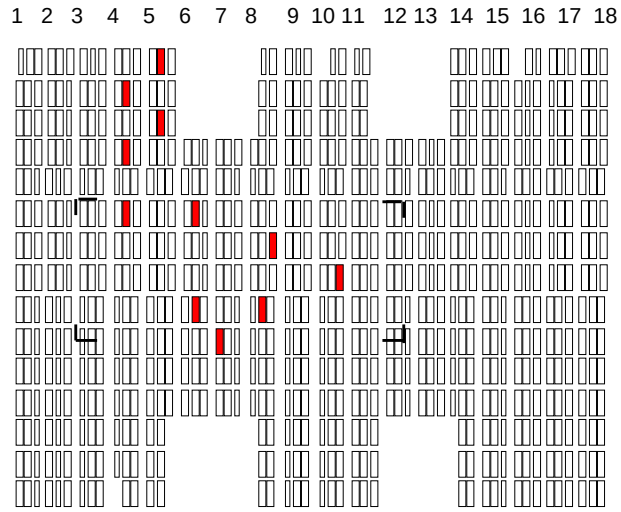

PPI sector

Identified defective tile ('old' inner wall)

* Used in BBQ validation tests
A. Seigneur et al, EPS'93
D. Guilhem et al Seville IAEA

TFTR

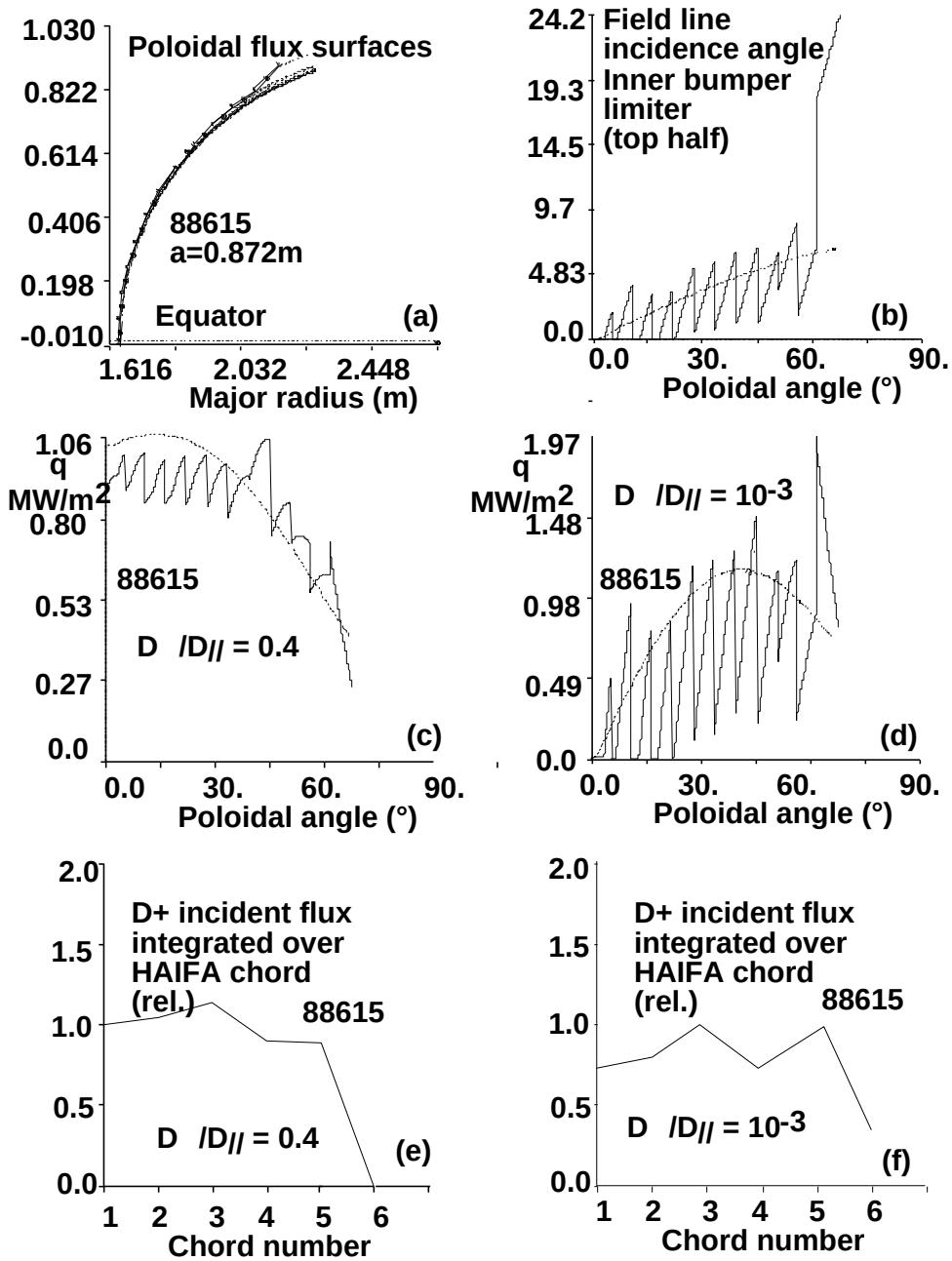
Poloidal flux surfaces
88615
a=0.872m
Equator
(a)
1.030
0.822
0.614
0.406
0.198
-0.010
1.616
2.032
2.448
Major radius (m)
Field line
incidence angle
Inner bumper
limiter
(top half)
(b)
24.2
19.3
14.5
9.7
4.83
0.0
0.0
30.
60.
90.
Poloidal angle (°)
q
MW/m2
88615
D /D// = 0.4
(c)
1.06
0.80
0.53
0.27
0.0
0.0
30.
60.
90.
Poloidal angle (°)
q
MW/m2
D /D// = 10-3
88615
(d)
1.97
1.48
0.98
0.49
0.0
0.0
30.
60.
90.
Poloidal angle (°)
D+ incident flux
integrated over
HAIFA chord
(rel.)
88615
D /D// = 0.4
(e)
2.0
1.5
1.0
0.5
0.0
1
2
3
4
5
6
Chord number
D+ incident flux
integrated over
HAIFA chord
(rel.)
88615
D /D// = 10-3
(f)
2.0
1.5
1.0
0.5
0.0
1
2
3
4
5
6
Chord number

Li intercalation and enhanced T retention

The Li coating technique was instrumental in producing high performance in TFTR supershots

BBQ calculations show that Li deposition is co-localized with D/T and C deposition in the leading edge region of the inner limiter (right)

Recent measurements by H. Sugai and co-workers [1] find rapid diffusion of Li into bulk graphite, promptly after deposition (intercalation)

In earlier work, Sugai et al found increased retention of D in Li (up to 100% of Li density, as compared with ~ 40% of C density).

Thus, intercalation (local accumulation of Li) and enhanced retention of T in the retained Li may act together to further amplify the strong localization of T retention which was found in earlier modeling

Relative distribution of Li wall deposition
Shot 76528
22MW D-T supershot

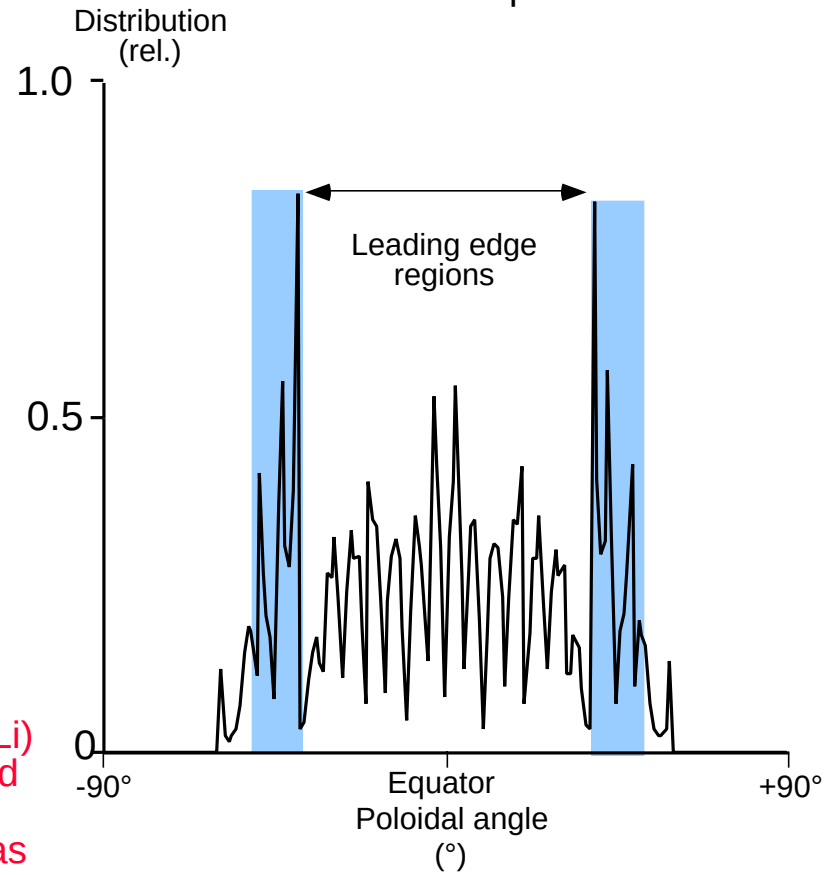

[1] N. Itou, H. Toyoda, K. Morita, H. Sugai
J. Nucl. Mater (to be publ. PSI 14, Rosenheim)

Ohmic discharges were used to prepare a saturated state, but the walls reverted to a pumping state with onset of ICRH*

Density behavior - OH saturation series
- with ergodic divertor (to maximize wall contact)

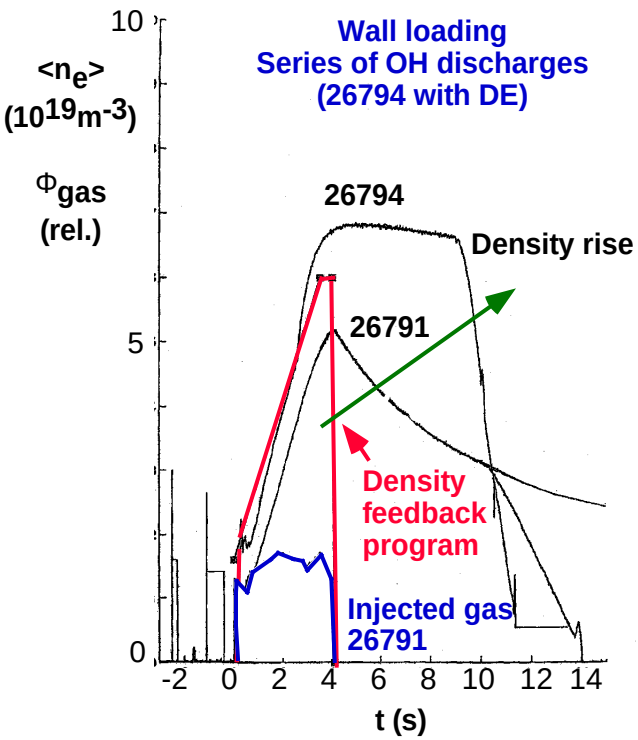

Density behavior - ICRH series
- outboard limiter

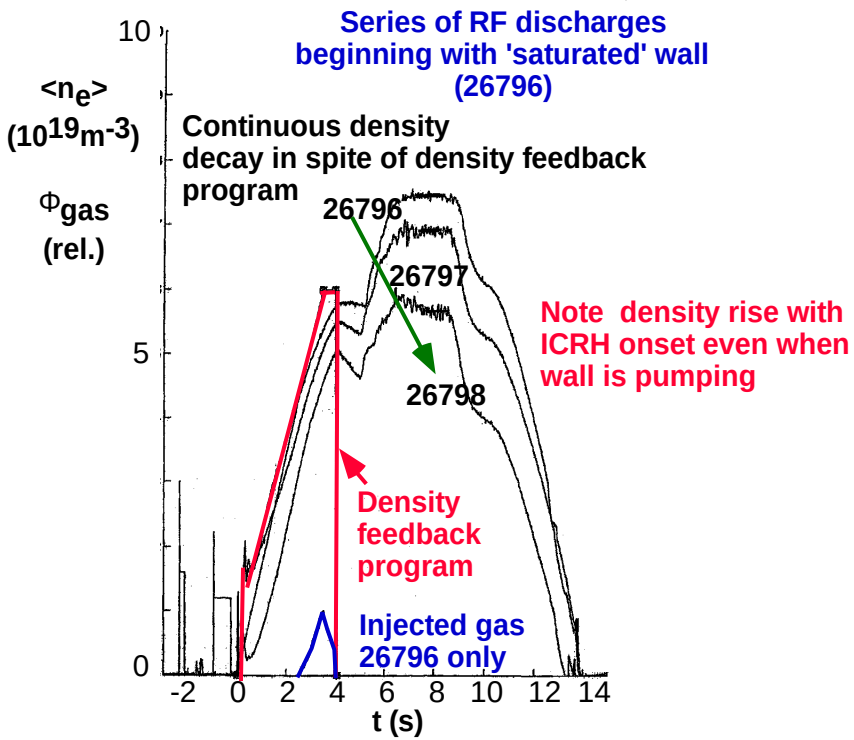

*C. Grisolia, J. Hogan, T. Hutter et al, to be published, J. Nucl. Mater.

ornl

Several models reproduce the *saturation -> pumping* transition which follows application of RF*

Wall modeling (WDIFFUSE) using CX fluxes (D-BBQ) with deposition range from TRIM

Ohmic phase

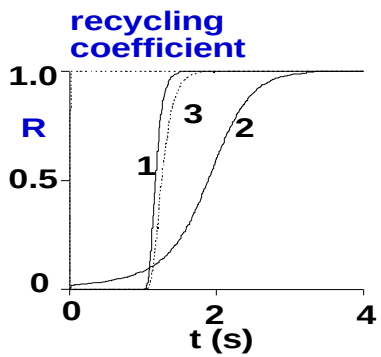

Several models predict the rapid (t_t~1.5 - 3 s) saturation in OH

Heating phase: 'hard' aC:D model

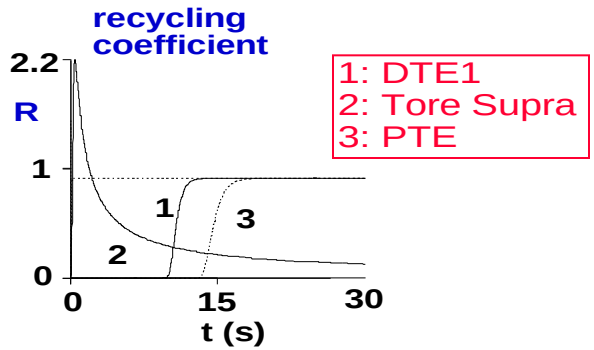

The models predict pumping at first, then longer transition (t_t~10 - 30 s) to saturation in RF-heating phase.

Heating phase: 'soft' aC:D model

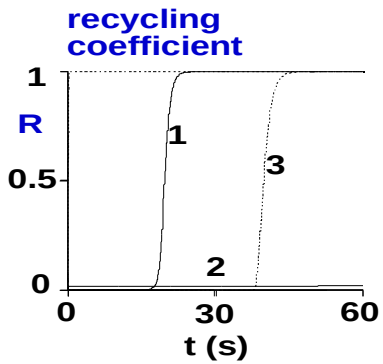

Greater D retention with 'soft' films increases the predicted transition time from pumping to saturation in heating phase. t_t~ 20-60s, near the observed values

1: DTE1
D. Hillis, J. Hogan, J. Ehrenberg et al Phys Plas 1999
2: Tore Supra
C. Grisolia, Th. Hutter, B. Pegourie et al, EPS '91
3: PTE
C. Grisolia, L. Horton, J. Ehrenberg, J Nucl Mater 1993

* C. Grisolia, J. Hogan, T. Hutter et al (to be published, J. Nucl. Mater.)

ornl

Possible effect of fast-ion ripple losses on impurity accumulation is related to development of ambipolarity condition in inherently non-axisymmetric configurations (e.g., stellarator, bumpy torus)

Time-dependence of electric fields in non-symmetric configurations was considered in:

"Ambipolar electric fields in stellarators"
D. E. Hastings, W. A. Houlberg, K.C. Shaing
Nuclear Fusion 25 (445) 1985

Multiple solutions (ion, electron branches) are possible.

The response time required to satisfy the unique radial ambipolarity constraint is determined by:

$$\frac{\varepsilon_{perp}}{e}\frac{d\Phi'}{dt} = \sum_{\alpha} Z_{\alpha}\,\Gamma_{\alpha}(\Phi')$$

Γ_{α} species α radial flux density

Φ electrostatic field

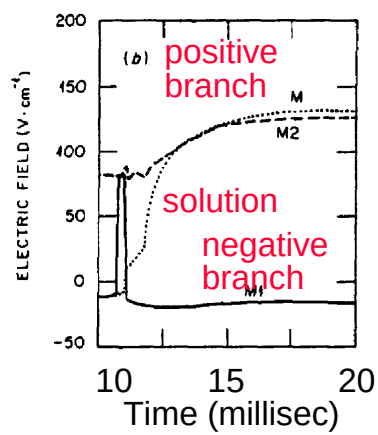

t_{resp} ~ 2 msec

Thus, can expect that, as non-axisymmetric (ripple) fluxes vary, impurity and deuterium fluxes will also vary quickly, to retain ambipolarity.

Discussion: status of predictive models

A hybrid 3D / 1D model, treating the SOL and ergodic edge region, reproduces several hitherto puzzling aspects of ergodic divertor performance:

- an unexplained peak in the (neon) poloidal emission profile was identified as a local 'plume'
- plume identification pointed to increased impurity efflux with increasing divertor current
- detailed comparison of edge influx and core confinement confirms the ELM-like screening effect

Intrinsic impurity generation processes are found, in some instances, to proceed at rates suggested by lab-scale experiments

- important role for T-dependent processes (chemical, RES) suggested for extended AT performance, in the absence of active cooling
- direct comparison of lab-scale and machine rates points to role of a-C:H films for intrinsic impurities

Experiments on species changeover (JET: D->T, T->D, D->H, H->D) and RF heating (TS) permit the formulation of working hypotheses for the process responsible for particle-induced desorption

- empirical rates agree with the Ehrenberg model
- there is a possible direct physical mechanism: chemical sputtering
- energetic CX spectrum and film characterization are key to determining the time scales for exchange

AT physics: impurity dynamics

- a plausible relation between sudden impurity expulsion and reduced ripple ion loss has been seen in AT (or near-AT) conditions

ornl